MITSUBISHI ELECTRIC RESEARCH LABORATORIES
https://www.merl.com

Closed-Form Local Stability of a Pressure-Phase-Coordinate Control-Volume Model

Qiao, Hongtao; Laughman, Christopher R.; Deshpande, Vedang M.; Bortoff, Scott A.

TR2026-134 September 22, 2026

Abstract

This paper studies the local stability of a pressure–phase-coordinate control-volume model for one-dimensional compressible flow. Using pressure and a generalized phase coordinate as the state variables, the model retains the essential effects of compressibility, phase change, flow restriction, and wall heat transfer while remaining simple enough for closed-form analysis. Starting from the mass and energy balances, explicit state equations are derived and linearized about an equilibrium operating point. The analysis yields a closed-form factorization of the Jacobian determinant, showing that saddle versus non-saddle behavior is governed by a single phase-coordinate sensitivity term in the energy balance. In strictly single-phase regions, and in the bulk of the two-phase region under the present approximation, the model is non-saddle. By contrast, sharp heat-transfer variation near phase boundaries can drive direct stable-to-saddle transitions. In a higher-pressure regime, the analysis also identifies conditions under which a Hopf candidate may arise. These results provide a simple and physically interpretable framework for understanding how heat transfer influences local stability in two-phase flow models.

Asian Modelica Conference 2026

Mitsubishi Electric Research Laboratories, Inc.
201 Broadway, Cambridge, Massachusetts 02139

Closed-Form Local Stability of a Pressure-Phase-Coordinate Control-Volume Model

Hongtao Qiao[1] Christopher R. Laughman[1] Vedang Deshpande[1] Scott A. Bortoff[1]

[1]Mitsubishi Electric Research Laboratories, Cambridge, MA, USA,
{qiao,laughman,deshpande,bortoff}@merl.com

Abstract

This paper studies the local stability of a pressure–phase-coordinate control-volume model for one-dimensional compressible flow. Using pressure and a generalized phase coordinate as the state variables, the model retains the essential effects of compressibility, phase change, flow restriction, and wall heat transfer while remaining simple enough for closed-form analysis. Starting from the mass and energy balances, explicit state equations are derived and linearized about an equilibrium operating point. The analysis yields a closed-form factorization of the Jacobian determinant, showing that saddle versus non-saddle behavior is governed by a single phase-coordinate sensitivity term in the energy balance. In strictly single-phase regions, and in the bulk of the two-phase region under the present approximation, the model is non-saddle. By contrast, sharp heat-transfer variation near phase boundaries can drive direct stable-to-saddle transitions. In a higher-pressure regime, the analysis also identifies conditions under which a Hopf candidate may arise. These results provide a simple and physically interpretable framework for understanding how heat transfer influences local stability in two-phase flow models.

Keywords: two-phase flow, control-volume model, pressure–phase coordinates, local stability, heat transfer, saddle instability

1 Introduction

Dynamic models are widely used in the simulation, analysis, and control of vapor-compression-based HVAC (Heating, Ventilation, Air-Conditioning) systems (Qiao et al. 2015). In practice, however, such models may exhibit pressure oscillations even under constant inputs, and the mechanism behind this behavior is not always clear. In particular, when the refrigerant moves across phase boundaries, the heat transfer coefficient may change sharply with phase state and introduce strong feedback into the system dynamics.

Fig. 1 shows a representative example from a cycle-level simulation, where the discharge pressure exhibits a sustained oscillation under constant inputs. Although this behavior can be observed numerically, its origin is difficult to identify directly from the full cycle model.

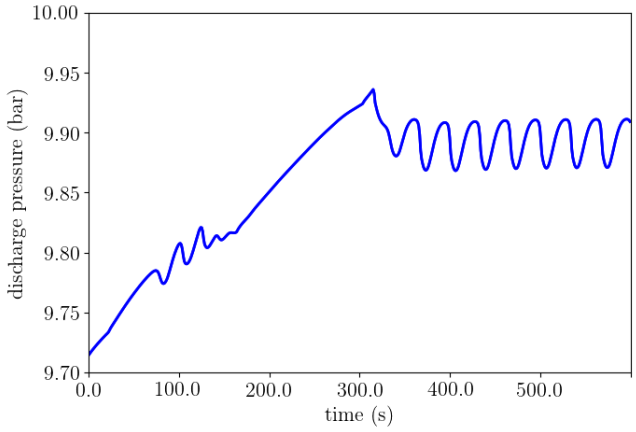

Figure 1. Oscillatory discharge-pressure behavior in a cycle-level simulation under constant inputs (Laughman and Qiao 2018).

Two-phase flow systems are known to exhibit a wide range of static and dynamic instabilities, including Ledinegg instability, pressure-drop oscillations, density-wave oscillations, and other system-level oscillatory phenomena (Yadigaroglu 1981; Kakaç and Bon 2008; Ruspini et al. 2014). These mechanisms have been studied in many thermal-fluid systems, including boiling channels, boilers, evaporators, refrigeration systems, and heat-pump components (Eborn and Åström 2000; Qiao and Laughman 2021). In this literature, stability is often determined by the interaction among pressure-drop characteristics, distributed transport delays, compressible volumes, phase-change dynamics, and external hydraulic boundary conditions.

The oscillation shown in Fig. 1 is related to this broader class of two-phase-flow stability problems, but the objective of the present paper is more local. Rather than analyzing a complete flow loop or a particular system-level instability mode, we study the local stability of a single pressure–phase-coordinate control-volume model coupled to an outlet flow relation. This reduced setting allows the effects of compressibility, phase change, flow restriction, and phase-dependent heat-transfer feedback to be isolated in closed form.

This local viewpoint is closely tied to the structure of detailed HVAC cycle models. Their dominant dynamics are often represented by finite-volume heat-exchanger models built from sequences of control volumes and flow

models. Such models capture the fluid and thermal dynamics well, but their complexity makes theoretical stability analysis difficult. As a result, even when oscillations are observed in simulation, it is not easy to determine whether they arise from flow restriction, thermodynamic sensitivities, heat-transfer closure, or the interaction of these effects.

The motivation of the present work is therefore to study this local feedback structure in a simpler analytical setting. The reduced model retains the essential mechanisms of compressibility, phase change, flow restriction, and heat-transfer feedback, while remaining simple enough for closed-form analysis. This viewpoint is also relevant beyond the reduced model itself, because many distributed heat-exchanger and cycle models are assembled from repeated control volumes coupled through flow restrictions. The present analysis should therefore be interpreted as a local mechanism study: it does not attempt to reproduce the full system dynamics, but instead isolates a compact feedback structure that may also govern instability in larger models.

For this purpose, the model is formulated in pressure and phase coordinate. The phase coordinate x coincides with vapor quality in the two-phase region and is extended continuously into the neighboring liquid and vapor regions through an enthalpy-based normalization. In these coordinates, the governing equations take the form of a compact second-order nonlinear system.

Within this framework, the paper develops closed-form local stability conditions for the pressure–phase-coordinate model. In particular, the analysis shows that local saddle versus non-saddle behavior is controlled by a single phase-coordinate sensitivity term in the energy balance, which directly links stability loss to sharp heat-transfer variation near phase boundaries. Representative simulation cases are then used to verify the resulting regime picture.

The remainder of the paper is organized as follows. Section 2 derives the pressure–phase-coordinate control-volume model. Section 3 develops the local stability conditions and their regime interpretation. Section 4 presents simulation cases that verify the analytical predictions. Section 5 concludes the paper.

2 Model Formulation

This section derives a control-volume model for one-dimensional compressible flow using pressure p and phase coordinate x as the state variables. The cross-sectional area is assumed constant, while gravitational force and axial heat conduction are neglected. The control volume is further assumed to remain in local thermodynamic equilibrium, so that thermodynamic properties can be parameterized by p and x (Laughman et al. 2026).

2.1 Definition of the phase coordinate

The state variable x is defined as vapor quality in the two-phase region. To extend the phase coordinate to single-phase regions, the same enthalpy-based normalization is continued outside the interval $[0,1]$ using the local saturation liquid and vapor enthalpies at the same pressure. Specifically, in the two-phase region,

$$x = \frac{h - h_{\mathrm{sat,liq}}(p,h)}{h_{\mathrm{sat,vap}}(p,h) - h_{\mathrm{sat,liq}}(p,h)}, \tag{1}$$

which reduces to the standard vapor-quality definition. In the vapor region, x is extended as

$$x = \frac{h - h_{\mathrm{dew,liq}}(p)}{h_{\mathrm{dew,vap}}(p) - h_{\mathrm{dew,liq}}(p)}, \tag{2}$$

and in the liquid region, x is extended as

$$x = \frac{h - h_{\mathrm{bub,liq}}(p)}{h_{\mathrm{bub,vap}}(p) - h_{\mathrm{bub,liq}}(p)}. \tag{3}$$

For a pure fluid, the same saturation-enthalpy difference may be used as the denominator in Equations (1)–(3). The separate bubble- and dew-based expressions are retained here because the formulation is also intended for refrigerant mixtures, for which the corresponding equilibrium liquid and vapor reference states generally have different phase compositions and enthalpy differences.

With this definition, $x = 0$ and $x = 1$ remain aligned with the saturated-liquid and saturated-vapor boundaries, respectively, while $x < 0$ represents liquid states and $x > 1$ represents vapor states. Thus, x serves as a continuous phase-coordinate across liquid, two-phase, and vapor regions. Outside the two-phase region, x should be interpreted as a generalized phase-coordinate rather than as a physical vapor mass fraction.

This extension is consistent with the two-phase definition because the normalization is based on the same local saturation reference states used to define vapor quality inside the two-phase region. As a result, the coordinate system remains continuous across the phase boundaries and is convenient for both model formulation and local stability analysis. In particular, it allows the same reduced-order state-space structure to be used when discussing the behavior near the liquid-to-two-phase and vapor-to-two-phase transitions.

Fig. 2 illustrates this construction schematically in the p–h plane. Inside the dome, the dashed green curves denote constant values of the phase coordinate x, which coincide with the conventional vapor quality. Outside the dome, the same normalization extends x continuously into the liquid region ($x < 0$) and vapor region ($x > 1$). The dashed black curve marks the locus along which $h_p = (\partial h/\partial p)_x$ changes sign. Importantly, this is not a single pressure level: the location of the sign change depends on the constant-x trajectory. This distinction will be used later when discussing bulk two-phase and vapor-region stability.

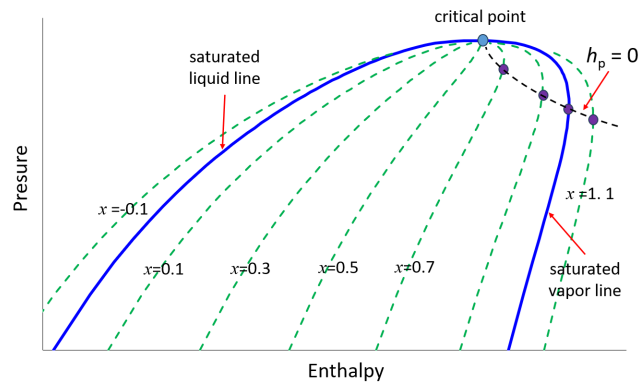

Figure 2. Schematic p–h representation of the extended phase coordinate x.

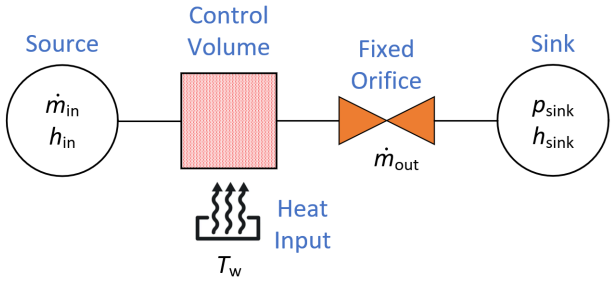

Figure 3. Control-volume model with inlet flow, fixed-orifice outlet, and wall heat input.

2.2 Governing equations

Fig. 3 shows the considered control volume. The inlet is characterized by mass flow rate $\dot{m}_{\text{in}}$ and specific enthalpy h_{in}, the outlet is connected to a pressure sink p_{sink} through a fixed orifice, and the wall exchanges heat with the fluid through a heat-transfer coefficient α, area A, and wall temperature T_w.

A convenient notation is to define the thermodynamic derivatives with respect to the independent variables p and x as

$$\rho_p = \left(\frac{\partial \rho}{\partial p}\right)_x, \qquad \rho_x = \left(\frac{\partial \rho}{\partial x}\right)_p, \tag{4}$$

$$h_p = \left(\frac{\partial h}{\partial p}\right)_x, \qquad h_x = \left(\frac{\partial h}{\partial x}\right)_p. \tag{5}$$

Here, ρ denotes fluid density and h denotes specific enthalpy. With these definitions, the mass and energy balances for the control volume can be written in compact form as

$$\begin{bmatrix} \rho_p & \rho_x \\ \rho h_p - 1 & \rho h_x \end{bmatrix} \begin{bmatrix} \dot{p} \\ \dot{x} \end{bmatrix} = \frac{1}{V} \begin{bmatrix} S_M \\ S_E \end{bmatrix}, \tag{6}$$

where V is the control-volume size, S_M is the net mass source term, and S_E is the energy source term.

Equation (6) is the key reduced storage relation of the model. The left-hand side captures how variations in pressure and phase coordinate affect density and enthalpy inside the control volume through thermodynamic sensitivities. The right-hand side contains the external forcing through the net mass and energy exchange. In this way, the model preserves the essential coupling between compressibility and phase change in a compact form.

The mass source term represents the net mass accumulation rate

$$S_M = \dot{m}_{\text{in}} - \dot{m}_{\text{out}}, \tag{7}$$

where the outlet flow is determined from a fixed-orifice relation

$$\dot{m}_{\text{out}} = \frac{\dot{m}_0}{(\Delta p_0)^{1/2}} (p - p_{\text{sink}})^{1/2}. \tag{8}$$

Equation (8) links the control-volume pressure to the downstream sink condition. The quantity K_p, introduced later, may be interpreted as the sensitivity of the outlet mass flow to pressure and therefore reflects the dynamic effect of the outlet restriction.

The energy source term consists of the inlet enthalpy flow and the external heat input,

$$S_E = \dot{m}_{\text{in}}(h_{\text{in}} - h) + \alpha A(T_w - T). \tag{9}$$

Equation (9) contains two distinct mechanisms. The first term represents the net enthalpy transport into the control volume after applying the well-mixed outlet condition $h_{\text{out}} = h$. Equivalently, it is the inlet enthalpy flow measured relative to the specific enthalpy of the fluid in the control volume. The second term describes heat transfer between the wall and the fluid. This decomposition is useful because the local stability result depends on how these two contributions vary with pressure and phase coordinate.

Solving (6) for $\dot{p}$ and $\dot{x}$ gives explicit state equations:

$$\dot{p} = \frac{\rho h_x S_M - \rho_x S_E}{\rho V h_x \left(\rho_p - \rho_x h_p h_x^{-1} + \rho^{-1} \rho_x h_x^{-1}\right)}, \tag{10}$$

$$\dot{x} = \frac{(1 - \rho h_p) S_M + \rho_p S_E}{\rho V h_x \left(\rho_p - \rho_x h_p h_x^{-1} + \rho^{-1} \rho_x h_x^{-1}\right)}. \tag{11}$$

These equations already show the main structure of the reduced model. Pressure and phase coordinate are not driven by separate balances; instead, both states respond to both S_M and S_E, and the coupling is weighted by the thermodynamic derivatives.

2.3 Characteristic speed and compact state-space form

To make the role of compressibility more transparent, the speed of sound c is rewritten in pressure–phase coordinates as (Qiao et al. 2023)

$$c = \left(\rho_p - \rho_x h_p h_x^{-1} + \rho^{-1} \rho_x h_x^{-1}\right)^{-1/2}. \tag{12}$$

It is convenient to define

$$\Upsilon \triangleq h_x^{-1}, \qquad \Lambda \triangleq \rho_x h_x^{-1} = \left(\frac{\partial \rho}{\partial h}\right)_p, \qquad \Phi \triangleq \frac{c^2}{\rho V}. \tag{13}$$

With the extended definition of x, one has $h_x > 0$, hence $\Upsilon > 0$, provided that the corresponding saturation-enthalpy differences are positive. Also, $\Phi > 0$. Moreover, at fixed pressure, increasing x moves the state toward the vapor side, so that $\rho_x < 0$. Therefore, $\Lambda < 0$.

Substituting the sound-speed expression into the state equations yields

$$\dot{p} = f_1(z,u) = \Phi\big[\rho S_M - \Lambda S_E\big], \tag{14}$$

$$\dot{x} = f_2(z,u) = \Phi\Upsilon\big[(1-\rho h_p)S_M + \rho_p S_E\big]. \tag{15}$$

The model is therefore a second-order nonlinear system with state vector

$$z = \begin{bmatrix} p \\ x \end{bmatrix}, \tag{16}$$

and input vector

$$u = \begin{bmatrix} \dot{m}_{\text{in}} & h_{\text{in}} & p_{\text{sink}} & T_w \end{bmatrix}^{\mathsf{T}}. \tag{17}$$

An equilibrium pair (z_e, u_e) satisfies

$$S_M(z_e,u_e) = 0, \qquad S_E(z_e,u_e) = 0. \tag{18}$$

Define the perturbations

$$\Delta z = z - z_e, \qquad \Delta u = u - u_e. \tag{19}$$

Linearizing the nonlinear system around (z_e, u_e) gives

$$\Delta\dot{z} = A\,\Delta z + B\,\Delta u, \tag{20}$$

where

$$A = \left.\frac{\partial f}{\partial z}\right|_{(z_e,u_e)}, \qquad B = \left.\frac{\partial f}{\partial u}\right|_{(z_e,u_e)}. \tag{21}$$

Since the local stability analysis depends only on the state Jacobian A, the full expressions for the entries of the input matrix B are omitted for brevity.

2.4 Source-term sensitivities and Jacobian structure

To express A compactly, define the source-term sensitivities at equilibrium. For the mass source term,

$$\frac{\partial S_M}{\partial p} = K_p, \qquad K_p = -\frac{\dot{m}_0}{2(\Delta p_0)^{1/2}}\frac{1}{\sqrt{p - p_{\text{sink}}}} < 0. \tag{22}$$

For the energy source term, define

$$\beta_p \triangleq \frac{\partial S_E}{\partial p}, \qquad \beta_x \triangleq \frac{\partial S_E}{\partial x}. \tag{23}$$

Since

$$S_E = \dot{m}_{\text{in}}(h_{\text{in}} - h) + \alpha A(T_w - T) \tag{24}$$

and $\alpha = \alpha(x)$, one obtains

$$\beta_p = -\dot{m}_{\text{in}} h_p - \alpha A T_p, \tag{25}$$

$$\beta_x = -\dot{m}_{\text{in}} h_x + \alpha_x A(T_w - T) - \alpha A T_x, \tag{26}$$

where

$$T_p = \left(\frac{\partial T}{\partial p}\right)_x, \qquad T_x = \left(\frac{\partial T}{\partial x}\right)_p, \qquad \alpha_x = \left(\frac{\partial \alpha}{\partial x}\right)_p. \tag{27}$$

Using these definitions, the Jacobian matrix can be written in the compact form

$$A = \Phi\begin{bmatrix} \rho K_p - \Lambda\beta_p & -\Lambda\beta_x \\ \Upsilon\big[(1-\rho h_p)K_p + \rho_p\beta_p\big] & \Upsilon\rho_p\beta_x \end{bmatrix}. \tag{28}$$

Equation (28) isolates the physical contributions that determine the local dynamics: outlet restriction through K_p, pressure-direction sensitivity of the energy source term through β_p, and phase-direction sensitivity through β_x.

2.5 Simplified heat-transfer model

To keep the local stability analysis analytically tractable, the heat-transfer coefficient α is approximated as a function of the phase coordinate x alone, as illustrated in Fig. 4. In general, however, α may also depend on pressure, wall temperature, mass flux, and other local flow variables. The present simplification is adopted because the goal of this paper is not to reproduce a detailed heat-transfer correlation, but to isolate the dominant phase-dependent variation that is most relevant to local stability near phase transitions.

Under this approximation, α is taken to be approximately constant in the liquid, bulk two-phase, and vapor regions, with representative values α_{liq}, α_{2ph}, and α_{vap}, respectively. Smooth blending is introduced in narrow transition regions near the liquid-to-two-phase and two-phase-to-vapor boundaries, so that α remains nearly constant over most of each phase region and varies rapidly only near the phase boundaries. This representation captures the main qualitative feature of practical heat-transfer correlations: the strongest phase-dependent variation often occurs near transitions between single-phase and two-phase conditions, whereas the variation within the bulk of each region is generally weaker.

Accordingly, $\alpha_x = d\alpha/dx = 0$ outside the transition regions. In the low-quality transition region, $\alpha_x > 0$ because α increases from α_{liq} to α_{2ph}. In the high-quality transition region, $\alpha_x < 0$ because α decreases from α_{2ph} to α_{vap}. As shown in the following section, this phase-boundary variation of α plays a central role in the onset of saddle instability.

Extension to general heat-transfer correlations. Although the regime interpretation developed below uses $\alpha = \alpha(x)$, the determinant simplification itself is not restricted to this assumption. For a more general heat-transfer correlation,

$$\alpha = \alpha(p, x, G, T_w, \ldots), \tag{29}$$

where G denotes the local mass flux, the pressure- and phase-direction sensitivities of the energy source term become

$$\beta_p = -\dot{m}_{\text{in}} h_p + A(T_w - T)\alpha_p - \alpha A T_p, \tag{30}$$
$$\beta_x = -\dot{m}_{\text{in}} h_x + A(T_w - T)\alpha_x - \alpha A T_x, \tag{31}$$

where

$$\alpha_p = \left(\frac{\partial \alpha}{\partial p}\right)_x, \qquad \alpha_x = \left(\frac{\partial \alpha}{\partial x}\right)_p \tag{32}$$

denote the complete local sensitivities of the heat-transfer coefficient.

In the present local analysis, the inlet mass flow is treated as an external input. Therefore, if the mass flux is determined directly from the prescribed inlet flow and flow area, it is held fixed when the state Jacobian is evaluated. In that case, mass-flux dependence changes the equilibrium value of α but does not introduce additional state derivatives. If a more general closure makes G state dependent, the derivatives in Eqs. (30) and (31) should instead be interpreted as total local sensitivities. For example,

$$\alpha_x^{\text{eff}} = \left(\frac{\partial \alpha}{\partial x}\right)_{p,G,T_w} + \left(\frac{\partial \alpha}{\partial G}\right)_{p,x,T_w} \left(\frac{\partial G}{\partial x}\right)_p. \tag{33}$$

With these complete sensitivities, the Jacobian retains the same structural form, and the determinant factorization derived in Section 3 remains

$$\det A = \frac{\Phi \Upsilon K_p}{V} \beta_x. \tag{34}$$

Thus, a more detailed heat-transfer correlation changes the numerical values of β_p and β_x and therefore shifts the trace and determinant boundaries. It does not, however, change the central structural result that saddle versus non-saddle behavior is governed by the phase-direction sensitivity of the complete energy source term.

3 Closed-Form Local Stability Conditions

Local stability is determined by the eigenvalues of the Jacobian matrix A. Because the linearized system is planar, its characteristic polynomial can be written as

$$\lambda^2 - \tau\lambda + \Delta = 0, \tag{35}$$

where

$$\tau = \operatorname{tr} A, \qquad \Delta = \det A. \tag{36}$$

The main point of this section is that, for the present pressure–phase-coordinate model, both Δ and τ admit physically interpretable forms. This makes the local stability conditions much more transparent than a direct numerical eigenvalue calculation.

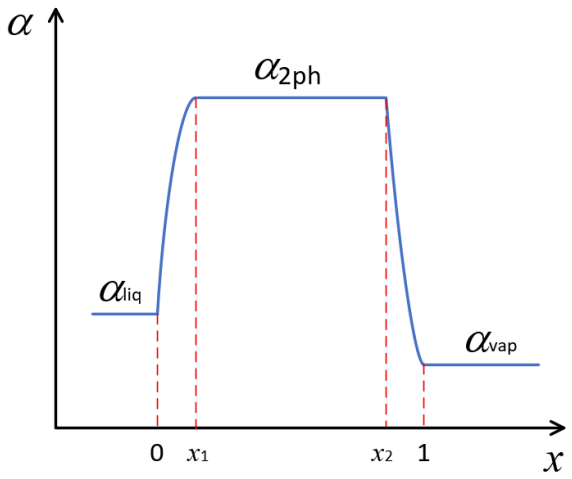

Figure 4. Heat transfer coefficient variations with extended phase coordinate x.

3.1 Determinant simplification

For the Jacobian above, the determinant admits the closed-form factorization. Starting from (28):

$$\begin{aligned}\Delta &= \Phi^2 \begin{vmatrix} \rho K_p - \Lambda\beta_p & -\Lambda\beta_x \\ \Upsilon\left[(1-\rho h_p)K_p + \rho_p\beta_p\right] & \Upsilon\rho_p\beta_x \end{vmatrix} \\ &= \Phi^2\Upsilon\beta_x\left[(\rho K_p - \Lambda\beta_p)\rho_p + \Lambda\big((1-\rho h_p)K_p + \rho_p\beta_p\big)\right] \\ &= \Phi^2\Upsilon K_p\beta_x\left[\rho\rho_p + \Lambda(1-\rho h_p)\right].\end{aligned}$$

The terms proportional to $\Lambda\rho_p\beta_p$ cancel. The remaining bracket is fixed by the sound-speed identity, since

$$\rho\rho_p + \Lambda(1-\rho h_p) = \rho\left(\rho_p - \Lambda h_p + \rho^{-1}\Lambda\right) = \rho c^{-2}.$$

Using $\Phi = c^2/(\rho V)$ then gives

$$\Delta = \frac{\Phi\Upsilon K_p}{V}\beta_x. \tag{37}$$

Since $\Phi > 0$, $\Upsilon > 0$, $K_p < 0$, and $V > 0$, the sign of Δ is governed entirely by the sign of β_x. Therefore,

$$\Delta > 0 \iff \beta_x < 0, \tag{38}$$
$$\Delta < 0 \iff \beta_x > 0, \tag{39}$$
$$\Delta = 0 \iff \beta_x = 0. \tag{40}$$

This is the key analytical simplification. The determinant test reduces to the sign of a single scalar coefficient associated with the phase-coordinate sensitivity of the energy source term. Through the expression for β_x, the determinant depends directly on the heat-transfer-coefficient gradient α_x in the transition regions, given that $T_x \geq 0$.

3.2 Trace condition

The trace of the Jacobian is

$$\tau = \Phi\left(\rho K_p - \Lambda\beta_p + \Upsilon\rho_p\beta_x\right). \tag{41}$$

Unlike the determinant, the trace does not reduce to a single sign-definite coefficient. Its sign depends on the operating condition through β_p and ρ_p, and therefore must in general be evaluated explicitly.

Accordingly, the determinant and trace play different roles: the determinant distinguishes saddle from non-saddle behavior through β_x, whereas the trace determines whether a non-saddle equilibrium is stable, unstable, or marginal.

3.3 General stability classification

For a second-order system, the Hurwitz criterion implies that the equilibrium is asymptotically stable if and only if

$$\Delta > 0, \qquad \tau < 0. \tag{42}$$

If $\Delta < 0$, the equilibrium is a saddle and is therefore necessarily unstable. If $\Delta > 0$ and $\tau = 0$, the equilibrium is marginal in the linear sense and is referred to here as a Hopf candidate. The boundary $\Delta = 0$ marks the transition between saddle and non-saddle behavior.

Thus, for the present model, the local stability problem separates naturally into two parts: a determinant test, governed entirely by β_x, and a trace test, which determines whether a non-saddle equilibrium is stable, unstable, or marginal.

3.4 Strictly single-phase equilibria

A useful simplification arises when the equilibrium lies strictly in the single-phase liquid or vapor regions. Under the present heat-transfer approximation, $\alpha_x = 0$ away from the blending zones. In that case,

$$\beta_x = -\dot{m}_{in} h_x - \alpha A T_x. \tag{43}$$

Since $h_x > 0$ and $T_x > 0$, one has $\beta_x < 0$, and therefore

$$\Delta = \frac{\Phi \Upsilon K_p}{V} \beta_x > 0. \tag{44}$$

Hence, strictly single-phase equilibria cannot be saddles under these conditions. The remaining classification is determined by the trace.

3.4.1 Liquid equilibria

In the strictly single-phase liquid region, we consider the operating regimes in which

$$K_p < 0, \qquad h_p > 0, \qquad T_p > 0, \qquad \rho_p < 0. \tag{45}$$

Then $\beta_p < 0$. From (41), the terms ρK_p and $-\Lambda\beta_p$ are negative, whereas $\Upsilon\rho_p\beta_x > 0$ because $\rho_p < 0$ and $\beta_x < 0$. Therefore, the sign of τ is not automatically negative in the general liquid-region case.

However, liquid is nearly incompressible in many operating conditions of interest, so that ρ_p is often small in magnitude. Under the approximation

$$\rho_p \approx 0, \tag{46}$$

the trace reduces to

$$\tau \approx \Phi\left(\rho K_p - \Lambda\beta_p\right). \tag{47}$$

Because $K_p < 0$, $\Lambda < 0$, and $\beta_p < 0$, both terms in (47) are negative, so $\tau < 0$. Together with (44), this implies local asymptotic stability in the strictly single-phase liquid region under the additional approximation $\rho_p \approx 0$.

3.4.2 Vapor equilibria

In the strictly single-phase vapor region, two subregimes may be distinguished.

Below the $h_p = 0$ locus. Consider the operating regime below the locus in the p–h plane where $h_p = (\partial h/\partial p)_x$ changes sign along constant-x trajectories (see Fig. 2). In this regime,

$$K_p < 0, \qquad h_p > 0, \qquad T_p > 0, \qquad \rho_p > 0. \tag{48}$$

Then $\beta_p < 0$. From (41), all three terms are negative:

$$\rho K_p < 0, \qquad -\Lambda\beta_p < 0, \qquad \Upsilon\rho_p\beta_x < 0.$$

Hence $\tau < 0$. Therefore, in this vapor-region subregime, the condition $\beta_x < 0$ implies not only $\Delta > 0$ but also $\tau < 0$, so the equilibrium is locally asymptotically stable.

Above the $h_p = 0$ locus. A second vapor-region subregime may arise above this locus. In that case, we may have

$$K_p < 0, \qquad h_p < 0, \qquad T_p > 0, \qquad \rho_p > 0. \tag{49}$$

Then the sign of $\beta_p = -\dot{m}_{in} h_p - \alpha A T_p$ is no longer fixed *a priori*, since the first term is positive while the second term remains negative. Consequently, $\beta_x < 0$ still guarantees $\Delta > 0$, but τ is no longer automatically negative and must be checked explicitly from (41).

In summary, strictly single-phase equilibria are always non-saddle under the present assumptions, because $\beta_x < 0$ implies $\Delta > 0$. In the liquid region, local asymptotic stability follows if the additional approximation $\rho_p \approx 0$ is adopted. In the vapor region, local asymptotic stability is automatic below the $h_p = 0$ locus, but must be checked explicitly once h_p becomes negative.

3.5 Two-phase equilibria

The two-phase region admits additional structure that is useful for interpreting the local stability conditions. Under the present heat-transfer approximation, the derivative $\alpha_x = d\alpha/dx$ vanishes over a large portion of the two-phase region and becomes significant only in narrow transition regions near the liquid-to-two-phase and two-phase-to-vapor boundaries. Accordingly, the bulk two-phase region and the phase-boundary regions should be treated separately.

Fig. 2 also indicates that the sign of h_p may change along a curve in the p–h plane rather than at a single pressure. Consequently, both the bulk two-phase region

and the high-quality transition region may admit lower-pressure and higher-pressure subregimes with different trace behavior.

For general two-phase equilibria, we retain

$$\beta_x = -\dot{m}_{in} h_x + \alpha_x A(T_w - T) - \alpha A T_x, \tag{50}$$

with

$$h_x > 0, \qquad T_x \geq 0. \tag{51}$$

The determinant is still given by (37), so the local saddle versus non-saddle character is determined entirely by the sign of β_x.

The trace is given by (41), with

$$\beta_p = -\dot{m}_{in} h_p - \alpha A T_p. \tag{52}$$

Define

$$\xi \triangleq \dot{m}_{in} h_x + \alpha A T_x > 0. \tag{53}$$

Then (50) becomes

$$\beta_x = -\xi + \alpha_x A(T_w - T). \tag{54}$$

The determinant changes sign when $\beta_x = 0$, which gives the critical gradient

$$\alpha_x^{\Delta} = \frac{\xi}{A(T_w - T)}. \tag{55}$$

The trace becomes zero when

$$\beta_x = \beta_x^{\tau} \triangleq \frac{\Lambda \beta_p - \rho K_p}{\Upsilon \rho_p}, \qquad \rho_p \neq 0. \tag{56}$$

Combining (54) and (56), the corresponding trace-zero boundary is

$$\alpha_x^{\tau} = \alpha_x^{\Delta} + \frac{\beta_x^{\tau}}{A(T_w - T)}. \tag{57}$$

Thus, α_x^{Δ} marks the saddle boundary, whereas α_x^{τ} marks the Hopf candidate boundary. If α_x^{τ} lies beyond α_x^{Δ} in the destabilizing direction, the equilibrium changes directly from stable to saddle and no Hopf boundary appears first. If α_x^{τ} is reached before α_x^{Δ}, then the system first crosses a trace-zero boundary while $\Delta > 0$, which is the linear signature of a Hopf candidate. Establishing a true finite-amplitude limit cycle would require further nonlinear analysis.

3.5.1 Bulk two-phase region

Over a large portion of the two-phase region, the heat transfer coefficient is approximated as constant with respect to x, so that

$$\alpha_x = 0. \tag{58}$$

Then $\beta_x = -\xi < 0$, and therefore $\Delta > 0$. Hence, equilibria in the bulk two-phase region are always non-saddle.

The trace behavior in the bulk two-phase region depends on the sign of h_p.

Below the $h_p = 0$ locus. In the lower-pressure part of the bulk two-phase region, that is, below the $h_p = 0$ locus, we observe

$$h_p > 0, \qquad \rho_p > 0, \qquad T_p > 0. \tag{59}$$

Then $\beta_p < 0$. Since $\beta_x < 0$, all three terms in (41) are negative, and therefore $\tau < 0$. Thus, bulk two-phase equilibria are locally asymptotically stable in this subregime.

Above the $h_p = 0$ locus. At higher pressures, above the $h_p = 0$ locus, we may instead have

$$h_p < 0, \qquad \rho_p > 0, \qquad T_p > 0. \tag{60}$$

Then β_p is no longer sign-definite. Therefore, while $\Delta > 0$ remains guaranteed, the sign of τ must be checked explicitly. In this higher-pressure bulk two-phase subregime, the equilibrium may therefore be stable, unstable, or marginal, but it cannot be a saddle.

3.5.2 Low-quality transition region

In the low-quality transition region, the heat transfer coefficient increases from its liquid-phase value to its two-phase value, and therefore

$$\alpha_x > 0. \tag{61}$$

For the operating regimes considered here, we further observe

$$h_p > 0, \qquad \rho_p > 0, \qquad T_p > 0, \tag{62}$$

which implies $\beta_p < 0$.

Substituting (61) into (54) shows that the gradient term is destabilizing only under heating,

$$T_w > T, \tag{63}$$

because then $\alpha_x A(T_w - T) > 0$. Under cooling ($T_w < T$), the same term is negative and therefore further decreases β_x, which reinforces stability.

Accordingly, in the low-quality region under heating, saddle instability may occur if

$$\alpha_x > \alpha_x^{\Delta}. \tag{64}$$

Moreover, because $\rho_p > 0$, $\beta_p < 0$, and $\Lambda < 0$, one has

$$\beta_x^{\tau} > 0. \tag{65}$$

Hence the trace-zero condition lies outside the non-saddle region $\beta_x < 0$. Equivalently, in the destabilizing direction,

$$\alpha_x^{\tau} > \alpha_x^{\Delta} \qquad (T_w > T), \tag{66}$$

so the equilibrium changes directly from stable to saddle. Therefore, in the low-quality transition region there is no Hopf boundary before saddle instability.

3.5.3 High-quality transition region

In the high-quality transition region, the heat transfer coefficient decreases from its two-phase value to its vapor-phase value, and therefore

$$\alpha_x < 0. \tag{67}$$

In this case, the gradient term in (54) is destabilizing only under cooling,

$$T_w < T, \tag{68}$$

because then $\alpha_x A(T_w - T) > 0$. Under heating ($T_w > T$), the same term is negative and again contributes to keeping $\beta_x < 0$.

Accordingly, in the high-quality region under cooling, saddle instability may occur if

$$\alpha_x < \alpha_x^{\Delta}, \tag{69}$$

since now both α_x and α_x^{Δ} are negative.

The trace behavior in the high-quality region depends on the sign of h_p.

Lower-pressure subregime ($h_p > 0$). In the lower-pressure part of the high-quality region, we may still have

$$h_p > 0, \qquad \rho_p > 0, \qquad T_p > 0. \tag{70}$$

Then $\beta_p < 0$, and as in the low-quality case one has $\beta_x^{\tau} > 0$. Hence the trace-zero boundary again lies beyond the saddle boundary in the destabilizing direction. Equivalently,

$$\alpha_x^{\tau} < \alpha_x^{\Delta} \qquad (T_w < T), \tag{71}$$

so the equilibrium changes directly from stable to saddle as α_x becomes more negative. Therefore, no Hopf boundary appears before saddle instability in this subregime.

Higher-pressure subregime ($h_p < 0$). At sufficiently high pressures, above the pressure at which the slope of the saturated-vapor line in the p–h plane changes sign, the constant-x pressure derivative of enthalpy may become negative:

$$h_p < 0, \qquad \rho_p > 0, \qquad T_p > 0. \tag{72}$$

In this case, the pressure sensitivity of the energy balance,

$$\beta_p = -\dot{m}_{\mathrm{in}} h_p - \alpha A T_p,$$

is no longer sign-definite. The first term is now positive, while the second term remains negative. Therefore, higher pressure does not by itself imply a Hopf-type loss of stability; it only makes such a possibility available if h_p is sufficiently negative.

The determinant condition is unchanged: the equilibrium is non-saddle only when

$$\Delta > 0 \quad \Longleftrightarrow \quad \beta_x < 0.$$

A Hopf candidate can occur only if the trace-zero boundary lies inside this non-saddle region. Since

$$\beta_x^{\tau} = \frac{\Lambda \beta_p - \rho K_p}{\Upsilon \rho_p},$$

the necessary condition for a Hopf candidate is

$$\beta_x^{\tau} < 0. \tag{73}$$

Using $\Upsilon > 0$, $\rho_p > 0$, $K_p < 0$, and $\Lambda < 0$, this condition is equivalent to

$$\beta_p > \frac{\rho K_p}{\Lambda}. \tag{74}$$

Because both K_p and Λ are negative, the right-hand side of (74) is positive. Thus β_p must not only become positive; it must become sufficiently positive. Substituting the definition of β_p, this requirement can be written as

$$-\dot{m}_{\mathrm{in}} h_p - \alpha A T_p > \frac{\rho K_p}{\Lambda}, \tag{75}$$

or equivalently,

$$h_p < -\frac{1}{\dot{m}_{\mathrm{in}}} \left(\alpha A T_p + \frac{\rho K_p}{\Lambda} \right). \tag{76}$$

Equation (76) shows that a Hopf candidate requires a rather restrictive condition: h_p must be sufficiently negative so that the pressure-induced enthalpy feedback overcomes both the stabilizing temperature-sensitivity term and the additional positive threshold imposed by the trace condition.

Consequently, three cases are possible in this higher-pressure subregime:

- If $\beta_x^{\tau} > 0$, the trace-zero boundary lies outside the non-saddle region. The equilibrium therefore remains stable until the determinant changes sign, and the loss of stability occurs through the saddle boundary.
- If $\beta_x^{\tau} = 0$, the trace-zero and determinant-zero boundaries coincide. This gives a codimension-two threshold at which $\tau = 0$ and $\Delta = 0$ occur simultaneously.
- If $\beta_x^{\tau} < 0$, the trace-zero condition is reached while $\Delta > 0$. In this case, the equilibrium crosses a Hopf candidate boundary before it reaches the saddle boundary.

For the high-quality transition under cooling, $T_w < T$, the destabilizing direction corresponds to α_x decreasing from zero toward more negative values. The determinant-zero boundary is reached at α_x^{Δ}, while the trace-zero boundary is reached at α_x^{τ}. Since the boundary closer to zero is encountered first, the ordering determines the transition sequence:

$$\alpha_x^{\tau} > \alpha_x^{\Delta} \implies \text{stable} \rightarrow \text{Hopf candidate} \rightarrow \text{saddle},$$

$$\alpha_x^\tau = \alpha_x^\Delta \implies \text{coincident trace/determinant boundary},$$
$$\alpha_x^\tau < \alpha_x^\Delta \implies \text{stable} \to \text{saddle}.$$

Equivalently, in this cooling case a Hopf candidate can occur only when the trace-zero boundary is reached before the determinant-zero boundary as α_x moves in the destabilizing direction. Here the term "Hopf candidate" is used only in the linearized sense ($\Delta > 0, \tau = 0$). Establishing a true Hopf bifurcation, and hence the existence and stability of a self-sustained limit cycle, would require further nonlinear analysis, such as checking the transversality condition and the first Lyapunov coefficient.

3.5.4 Summary regime map

The results above can be summarized as a regime map in the p–h plane, shown schematically in Fig. 5. The map organizes the local stability picture according to phase region, the sign of α_x, the destabilizing heat-transfer direction, and the resulting local mechanism.

In the strictly single-phase liquid region, $\alpha_x = 0$, so $\beta_x < 0$ and the equilibrium is non-saddle under the present approximation. In the single-phase vapor region below the $h_p = 0$ locus, $\alpha_x = 0$ likewise gives $\Delta > 0$, and the trace is automatically negative in the operating regime considered here, so the equilibrium is locally asymptotically stable. Above the $h_p = 0$ locus, the equilibrium remains non-saddle, but the trace must be checked explicitly because β_p is no longer sign-definite.

Within the two-phase region, the bulk regime is characterized by $\alpha_x = 0$, so the equilibrium is again non-saddle. Below the $h_p = 0$ locus, the trace is negative and the equilibrium is locally asymptotically stable. At higher pressures, however, the trace must again be checked explicitly. By contrast, the low-quality and high-quality transition regions are distinguished by nonzero heat-transfer gradients. In the low-quality transition region, $\alpha_x > 0$, and the destabilizing situation is heating, $T_w > T$. In the high-quality transition region, $\alpha_x < 0$, and the destabilizing situation is cooling, $T_w < T$. In both cases, sufficiently steep phase-boundary variation of the heat transfer coefficient can drive a direct stable-to-saddle transition through the determinant boundary.

A further distinction arises in the higher-pressure high-quality regime, where $h_p < 0$ and β_p is no longer sign-definite. In that case, the trace-zero boundary may in principle be reached before the determinant-zero boundary, so a Hopf candidate becomes theoretically possible. As discussed above, this requires more restrictive conditions than the ordinary determinant-driven saddle transition and, in the present model, appears to require operating points close to the critical region.

4 Modelica-Based Case Studies and Numerical Verification

This section presents Modelica-based case studies that verify the analytical stability conditions developed in Section 3. The four cases are selected to mirror the regime structure summarized in Fig. 5, and their schematic locations in the p–h plane are shown in Fig. 6: Case 1 considers the bulk two-phase stable regime, Cases 2 and 3 examine the low-quality and high-quality transition regions where determinant-driven saddle instability may occur, and Case 4 probes the higher-pressure regime in which a Hopf candidate is theoretically possible.

Table 1. Model parameters common to all case studies.

Parameter	Value
Refrigerant	R410A
Control-volume size V [m^3]	3.927e-5
Heat-transfer area A [m^2]	1.571e-2
Reference mass flow rate $\dot{m}_0$ [kg/s]	0.02
Reference pressure drop Δp_0 [Pa]	1e3
$\dot{m}_{\text{in}}$ [kg/s]	0.02
α_{liq} [W/(m^2 K)]	600
α_{vap} [W/(m^2 K)]	300
Low-quality blending interval	[0, 0.05]
High-quality blending interval	[0.95, 1]

4.1 Implementation and evaluation procedure

The refrigerant is taken to be R410A, and all thermodynamic properties and their derivatives are evaluated from the same property model used throughout the paper. The model is implemented in Modelica and simulated in Dymola. For simplicity, the phase-boundary variation of the heat-transfer coefficient is represented by linear blending in the low-quality and high-quality intervals.

For each case, the control-volume geometry, inlet conditions, outlet restriction, and wall temperature are fixed so that an equilibrium point (p_e, x_e) exists. The principal model parameters common to all four cases are listed in Table 1, while the case-dependent heat-transfer coefficients and operating conditions are summarized in Table 2.

The local quantities

$$h_p, \quad h_x, \quad \rho_p, \quad \rho_x, \quad T_p, \quad T_x, \quad \beta_p, \quad \beta_x, \quad \Delta, \quad \tau$$

are then evaluated at the equilibrium. A small perturbation is subsequently applied to the state, and the nonlinear response is compared with the local prediction from the Jacobian.

4.2 Case 1: Stable equilibrium in the bulk two-phase region

The first case considers an equilibrium located in the bulk two-phase region, away from the phase boundaries. Under the present heat-transfer approximation, this corresponds to $\alpha_x = 0$. The selected equilibrium lies below the $h_p = 0$ locus, so that $h_p > 0$, $\rho_p > 0$, and $T_p > 0$. As shown in Section 3, this implies $\beta_x < 0$, hence $\Delta > 0$, and the trace is also negative. The equilibrium is therefore predicted to be locally asymptotically stable.

The numerical simulations confirm this prediction. Small perturbations in both p and x decay in time, and the trajectory returns to the original equilibrium. Fig. 7 shows

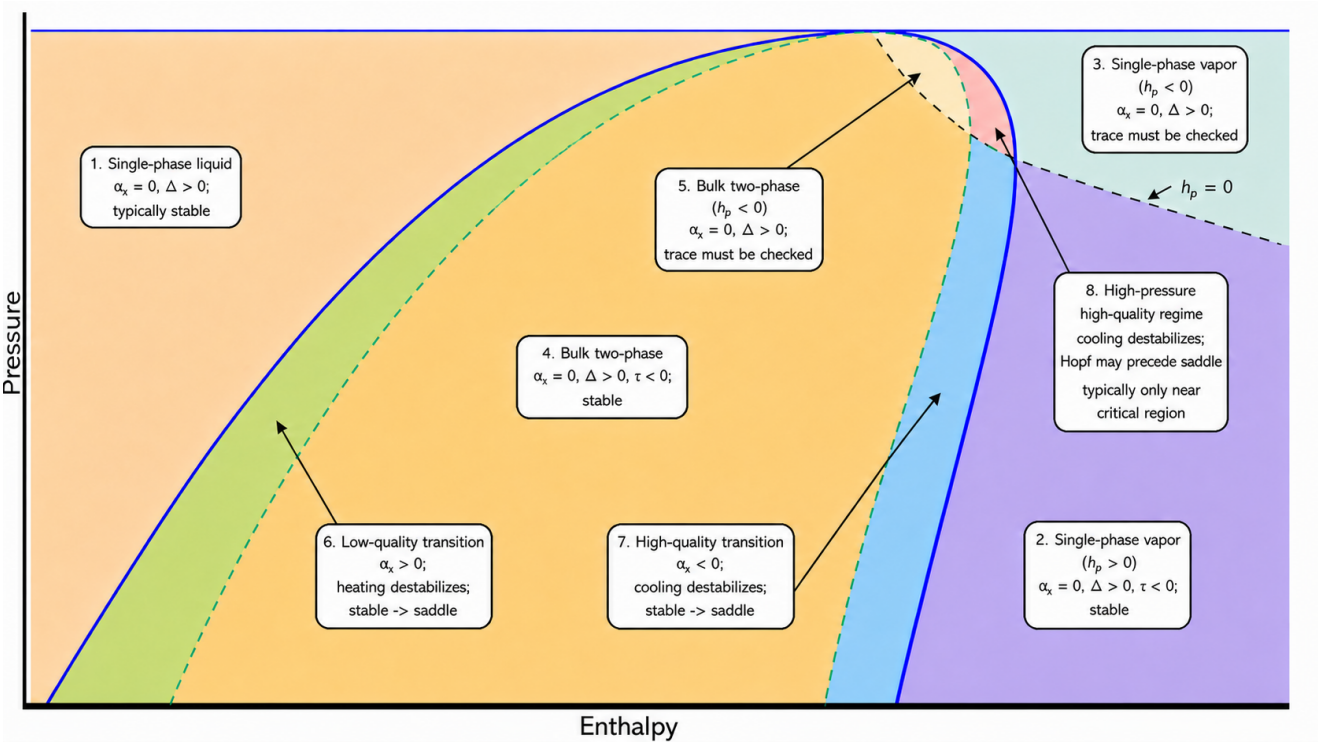

Figure 5. Summary regime map of the local stability mechanisms predicted by the closed-form analysis.

Table 2. Case-dependent operating conditions and equilibrium states.

Parameter	Case 1	Case 2	Case 3	Case 4
α_{2ph} [W/(m^2 K)]	1e4	3e3	3e3	6e3
h_{in} [kJ/kg]	237.15	192.6	423.8	404.0
p_{sink} [bar]	0.7	0.7	1.0	4.5
T_w [°C]	5	1	-1	62

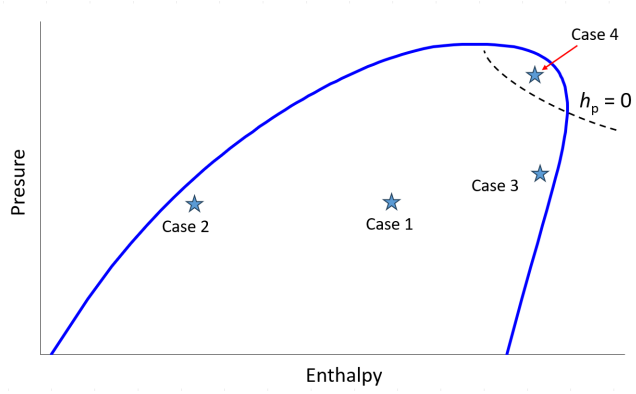

Figure 6. Schematic locations of the four simulation cases in the p–h plane.

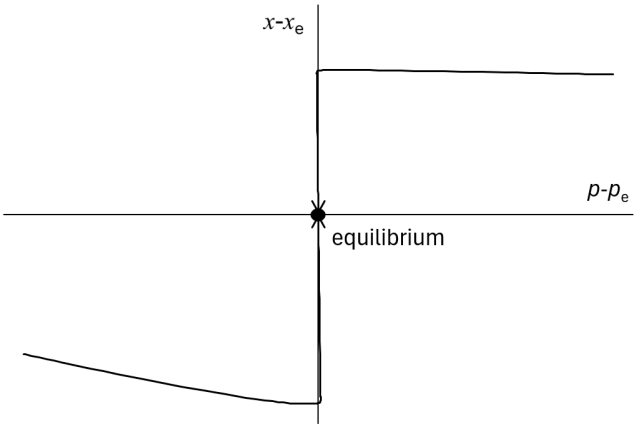

Figure 7. Phase portrait for Case 1 in the bulk two-phase region.

the corresponding phase portrait in the $(p - p_e,\ x - x_e)$ plane for two representative initial perturbations. In both cases, the trajectories converge back to the same equilibrium, confirming that the operating point is locally attracting.

The phase portrait also indicates a clear separation of time scales near the equilibrium. The trajectories approach the equilibrium much more rapidly in the pressure direction, whereas the phase coordinate relaxes more slowly. Thus, for this operating point, the pressure response is faster than the phase-coordinate response.

4.3 Case 2: Low-quality transition region under heating

The second case considers an equilibrium in the low-quality transition region, where the heat-transfer coefficient increases from its liquid-phase value to its two-phase value, so that $\alpha_x > 0$. The destabilizing situation is heating, $T_w > T$, because the gradient contribution $\alpha_x A(T_w - T)$ enters β_x with a positive sign. Under the sign pattern $h_p > 0$, $\rho_p > 0$, and $T_p > 0$, the analysis in Section 3 predicts that the trace remains negative throughout the non-saddle region. Hence, as α_x increases, the expected transition is a direct loss of local stability through the determinant boundary α_x^{Δ}, that is, from a stable equilibrium to a saddle.

To verify this prediction, the equilibrium is kept in the same low-quality region while the width of the linear blending interval is reduced in the Modelica implementation. This increases the local heat-transfer gradient without changing the thermodynamic regime. Three representative conditions are then considered: one below the determinant threshold, one near it, and one beyond it. Below the threshold, $\beta_x < 0$ and $\Delta > 0$, so the equilibrium remains locally asymptotically stable and a small perturbation returns to the original operating point. Near the threshold, β_x approaches zero and Δ becomes small, so the recovery becomes slow. Beyond the threshold, $\beta_x > 0$ and $\Delta < 0$, and the original equilibrium becomes a saddle.

Fig. 8 summarizes the resulting nonlinear behavior. The time responses in Fig. 8(a) show the three regimes clearly: return to the original equilibrium below the threshold, slow recovery near the threshold, and loss of attraction beyond the threshold. The phase portrait in Fig. 8(b) shows that, after the determinant threshold is crossed, the original equilibrium at (p_e, x_e) no longer attracts nearby trajectories. Instead, the trajectories separate into two groups and converge to an upper or lower attractor. The dashed line indicates the approximate basin boundary inferred from the simulations. In this case, the boundary is not aligned with the coordinate axes, so both pressure and phase-coordinate perturbations influence which attractor is reached.

Thus, Case 2 confirms the determinant-driven stable-to-saddle transition predicted analytically for the low-quality transition region under heating.

4.4 Case 3: High-quality transition region under cooling

The third case is constructed in a manner parallel to Case 2, but in the high-quality transition region, where the heat-transfer coefficient decreases from its two-phase value to its vapor-phase value, so that $\alpha_x < 0$. The destabilizing situation is now cooling, $T_w < T$, because the gradient contribution $\alpha_x A(T_w - T)$ is then again positive. As discussed in Section 3, sufficiently large negative heat-transfer gradients can drive the determinant through zero and cause the original equilibrium to lose local attraction.

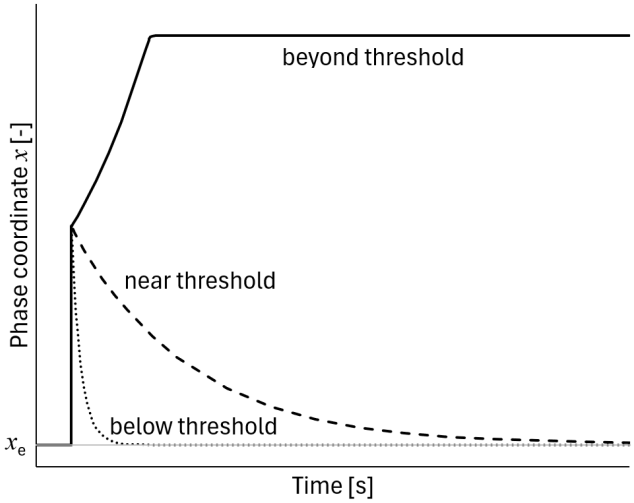

(a) Time responses of x for representative operating conditions.

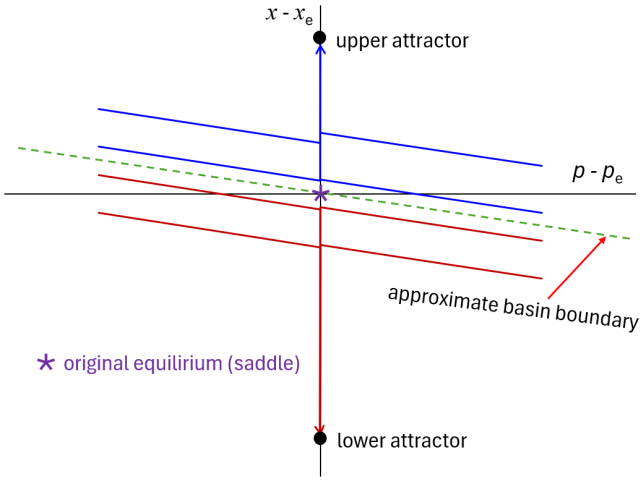

(b) Phase portrait in the $(p - p_e,\ x - x_e)$ plane for a beyond-threshold condition.

Figure 8. Case 2 in the low-quality transition region under heating.

The main point of this case, however, is not merely the threshold crossing itself, but the richer nonlinear behavior that appears beyond it. In the simulations considered here, a beyond-threshold parameter setting is chosen and the model is initialized with two nearby but distinct phase-coordinate perturbations while all other parameters are kept unchanged. Fig. 9 shows the corresponding time responses of the phase coordinate. Although both trajectories start in the neighborhood of the same original equilibrium x_e, they evolve toward different final operating points.

This result indicates that the nonlinear system admits multiple accessible steady equilibria under the same parameter setting. In other words, once the original equilibrium has lost local attraction, the long-time behavior is no longer determined by the parameters alone, but also by the initial condition. The upper and lower final states shown in Fig. 9 therefore represent two distinct attractors in the

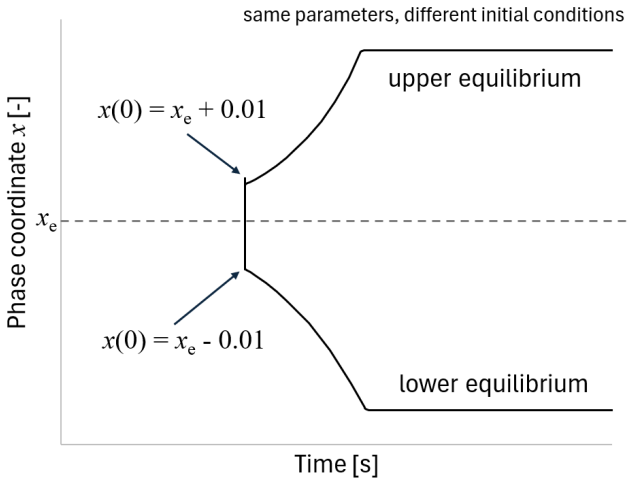

Figure 9. Case 3: time responses of the phase coordinate for identical parameters and different initial conditions.

beyond-threshold regime.

Thus, Case 3 confirms the same determinant-driven loss of local stability identified analytically for the high-quality transition region under cooling. In particular, the coexistence of multiple attractors implies multiple basins of attraction and shows that the post-threshold dynamics cannot be characterized by a single attracting operating point.

4.5 Case 4: Higher-pressure regime

The fourth case examines the higher-pressure regime in which $h_p < 0$, so that β_p is no longer sign-definite. In this subregime, the determinant is still controlled by β_x, but the trace must be checked explicitly. As shown in Section 3, this change in trace structure opens the possibility that the trace-zero boundary may be reached before the determinant-zero boundary. Accordingly, three scenarios are theoretically possible: a direct stable-to-saddle transition, a coincident trace-zero and determinant-zero boundary, or a Hopf candidate if the trace-zero boundary is encountered while $\Delta > 0$.

The purpose of this case is therefore not simply to reproduce another stable-to-saddle transition, but to assess whether the higher-pressure regime can bring the trace-zero boundary α_x^τ close to the determinant-zero boundary α_x^Δ. To this end, the operating point is moved into a region where $h_p < 0$, and the corresponding local stability quantities and nonlinear response are then assessed.

The numerical exploration shows that, in the operating range considered here, the determinant-zero boundary is reached well before the trace-zero boundary. Equivalently, as α_x decreases from zero toward more negative values, α_x^Δ is encountered before α_x^τ. In this cooling case, this corresponds to

$$\alpha_x^\tau < \alpha_x^\Delta < 0.$$

Bringing the two thresholds closer would require h_p to become sufficiently small and strongly negative, so that the pressure-induced enthalpy feedback makes β_p large enough to satisfy the trace-zero condition within the non-saddle region. In the present model, this appears to occur only very near the critical region. Thus, although a Hopf candidate is theoretically possible in the higher-pressure regime, the dominant numerically accessible mechanism in the present study remains the direct determinant-driven stable-to-saddle transition.

5 Conclusions

This paper developed a pressure–phase-coordinate control-volume model and derived closed-form local stability conditions for compressible two-phase flow. The main analytical result is that saddle versus non-saddle behavior is determined directly by the sign of β_x, the phase-coordinate sensitivity term in the energy balance.

The analysis shows that strictly single-phase equilibria and the bulk two-phase region are non-saddle under the present approximation. By contrast, the numerical case studies show that the dominant instability mechanism in the operating range considered here is localized near phase boundaries: sharp variation of the heat transfer coefficient near the liquid-to-two-phase and two-phase-to-vapor transitions can drive a direct stable-to-saddle transition.

The simulations further show that loss of local stability need not appear as unbounded divergence. Instead, the state may depart from the original equilibrium and converge to a different stable operating point, and in some beyond-threshold regimes multiple attractors may coexist.

A Hopf candidate is theoretically possible in a higher-pressure regime where $h_p < 0$ and β_p is no longer sign-definite, but this requires more restrictive conditions than the determinant-driven saddle transition and was not found to be the dominant behavior in the cases studied here.

From a modeling and control perspective, the derived stability conditions provide a compact local diagnostic for identifying sensitive operating regions in distributed thermal-fluid models. In particular, the sign of β_x can be monitored along a nominal operating trajectory to determine whether an individual control volume remains non-saddle or approaches a determinant-driven loss of local attraction. Operating points with β_x close to zero are of particular practical interest because the determinant becomes small, the local recovery becomes slow, and the model may become more sensitive to disturbances, parameter uncertainty, and numerical regularization. This information can support operating-envelope selection, heat-transfer-model regularization, spatial-discretization decisions, and gain-scheduled, supervisory, or optimization-based control design. The criterion should nevertheless be interpreted as a local screening tool rather than as a complete stability condition for the full vapor-compression cycle.

The present result is also qualitatively consistent with a common observation in cycle-level simulations, namely that oscillatory behavior is more often seen in the high-

pressure side than in the evaporating pressure. A possible reason is that condenser models often traverse a large portion of the two-phase region, including the phase-boundary transition regions identified here as locally destabilizing, whereas evaporator inlet states may already be beyond the low-quality transition region and therefore spend less of the evaporation process in that locally sensitive zone.

Although the analysis is carried out in pressure–phase coordinates, the same local instability mechanism is expected to persist in more conventional pressure–enthalpy formulations and in larger distributed models built from the same control-volume and flow-restriction ingredients.

References

Eborn, Jonas and Karl J. Åström (2000). "Modeling of a Boiler Pipe with Two-Phase Flow Instabilities". In: *Modelica Workshop 2000 Proceedings*. Lund, Sweden, pp. 79–88.

Kakaç, S. and B. Bon (2008). "A Review of Two-Phase Flow Dynamic Instabilities in Tube Boiling Systems". In: *International Journal of Heat and Mass Transfer* 51.3–4, pp. 399–433.

Laughman, Christopher and Hongtao Qiao (2018). "On Closure Relations for Dynamic Vapor Compression Cycle Models". In: *American Modelica Conference*.

Laughman, Christopher, Hongtao Qiao, Scott Bortoff, and Vedang Deshpande (2026). "On State Selection for Vapor Compression Cycle Models with Refrigerant Mixtures". In: *21st International Refrigeration and Air-Conditioning Conference at Purdue*.

Qiao, Hongtao, Vikrant Aute, and Reinhard Radermacher (2015). "Transient Modeling of a Flash Tank Vapor Injection Heat Pump System – Part I: Model Development". In: *International Journal of Refrigeration* 49, pp. 169–182. ISSN: 0140-7007.

Qiao, Hongtao, Takashi Kobayashi, Christopher Laughman, and Scott Bortoff (2023). "On the Characteristics of One-Dimensional Compressible Flow". In: *The 15th International Modelica Conference*.

Qiao, Hongtao and Christopher Laughman (2021). "Modeling and Analysis of Pressure Drop Oscillations in Horizontal Boiling Flow". In: *Proceedings of the 18th International Refrigeration and Air Conditioning Conference at Purdue*. Paper 2190.

Ruspini, Leonardo C., Christian P. Marcel, and Alejandro Clausse (2014). "Two-Phase Flow Instabilities: A Review". In: *International Journal of Heat and Mass Transfer* 71, pp. 521–548.

Yadigaroglu, G. (1981). "Two-Phase Flow Instabilities and Propagation Phenomena". In: *Thermal-Hydraulics of Two-Phase Systems for Industrial Design and Nuclear Engineering*. Ed. by J. M. Delhaye, M. Giot, and M. L. Riethmuller. New York: Hemisphere Publishing Corporation. Chap. 17.